# Axisymmetric Bluff-Body Drag Reduction Through Geometrical Modification

Floyd G. Howard* and Wesley L. Goodman*
*NASA Langley Research Center, Hampton, Virginia*

**The effect of shoulder radiusing and grooving (longitudinally and circumferentially) the afterbodies of bluff bodies to reduce the base drag at low speeds is investigated experimentally. Shoulder radii as large as 2.75 body diameters are examined. Reynolds number ($Re_D$) based on body diameter varied from 20,000 to 200,000. Results indicate that increasing the shoulder radius to 2.00 body diameters can reduce the drag levels to those of a streamline body having 67% greater fineness ratio. For the relatively sharp shoulder case, body drag reductions as large as 50 and 33% are obtained using circumferential or longitudinal grooves, respectively.**

## Nomenclature

$A$ = maximum body cross-sectional area
$a$ = groove depth measured on the downstream side of a circumferential rectangular groove
$b$ = width of circumferential rectangular groove
$C_D$ = drag coefficient based on body cross-sectional area
$D$ = body diameter, 6.081 cm
$h$ = height of trip wire
$\ell$ = body length, $\ell/D = 3$
$N$ = number of grooves
$p$ = pressure
$Re_D$ = freestream Reynolds number based on body diameter
$R_s$ = afterbody shoulder radius
$S$ = surface distance measured from first tangency point of shoulder (see Table 1)
$t$ = spacing between circumferential rectangular grooves
$U_\infty$ = freestream velocity
$V$ = body volume
$x$ = longitudinal distance from nose
$\theta_B$ = half-angle of conical afterbody, = 30 deg (Fig. 1)
$\theta_{BG}$ = angle between longitudinal V groove and body centerline, = 19.4 deg
$\theta_v$ = cross sectional included angle of longitudinal V groove, = 90 deg

*Subscripts*

SB = streamline body

## Introduction

FOR performance improvement and energy conservation, it is desirable to reduce the base drag of bluff bodies such as bombs, bullets, automobiles, trucks, buses, planetary-entry shapes, and the upswept fuselage of some military cargo aircraft. In recent years, as a result of dwindling petroleum resources, increased emphasis has been focused upon drag-reduction research for all forms of transportation. The drag on the aforementioned bodies is often dominated by base or afterbody flow-separation effects (i.e., form or pressure drag). Estimates[1] indicate that a 40% reduction in automobile aerodynamic drag would result in an increase in fuel economy on the order of 16%. By definition, bluff bodies have a low fineness ratio (i.e., on the order of 3 or less). It is possible to eliminate most flow separation and thereby obtain low drag coefficients even for such low fineness ratios by moving the maximum body thickness far forward and using a gradual afterbody closure. However, this approach typically does not provide sufficient volume for passengers, cargo, and motive power when the length is restricted. Therefore, ground transportation bodies are typically truncated rather sharply resulting in large form drag.

Several techniques are available for reducing bluff-body separation drag in the two-dimensional case, where the drag is quite high, primarily due to vortex shedding.[2] However, these two-dimensional techniques, which usually control or prevent vortex shedding, generally are not successful in the axisymmetric or fully three-dimensional base-separation case[3,4] where typically it has proven to be much more difficult to reduce base drag. Two nonpassive techniques successful in reducing flow separation in three-dimensional cases are blowing[5-12] (mass addition) or suction[10-13] (mass removal). Three-dimensional base flow separation can also be reduced by passive techniques such as boattailing and other geometrical modifications to the base region. A review of afterbody drag reduction through 1) shoulder radiusing,[14-19] 2) circumferential rectangular grooves,[20] and 3) longitudinal V grooves[18,21] has been conducted. The results are compared and reported herein.

## Experimental Apparatus

Experiments were conducted in the Langley 7×11-in. Low-Speed Wind Tunnel. A detailed description of this closed-loop tunnel may be found in Ref. 22. The tunnel was operated at stream velocities 5-45 m/s for the current study. The stream velocity and Reynolds number were determined from measurements with pitot-static pressure and total temperature probes at the entrance of the test section. Direct drag measurements were made with a floating-element balance which consisted of a strut-support assembly, an air bearing, and a force-measuring sensor. Flow-induced drag on the model was transmitted directly to the force-measuring sensor. Although this sensor was accurate to ±1%, repeated measurements of the drag on a streamlined body indicated 10% repeatability.

Reference 23 describes the basic flow-visualization technique utilized in the present study. A small vertical wire was coated with oil and heated to produce a sheet of closely spaced, thin, smoke filaments. A short-duration flash to freeze the motion was directed through the top of the tunnel

Received Oct. 31, 1984; revision received March 15, 1985. 

*Aerospace Engineer, Viscous Flow Branch, High-Speed Aerospace Division.

and the camera was pointed through the side of the tunnel. For some tests, a lateral cross section of the flow was desired. To obtain this, an array of several vertical smoke wires was placed laterally across the test section and the flash was adjusted to illuminate a thin lateral cross section. A small mirror positioned downstream of the illuminated cross section directed this view to a camera.

## Models

All models tested and reported herein were axisymmetric with a maximum body diameter of 6.081 cm. Examples of the four basic configurations tested are shown in Fig. 1. These models, which had a cross-sectional area of 29.03 $cm^2$ (4.5 $in.^2$), were originally designed for a larger facility; hence there is a blockage error on the order of 10% (determined from the method in Ref. 24, as well as recent measurements in a larger test section) in the present results. The actual drag would be lower than the data quoted herein due to this blockage; however, this correction should be approximately on the same order for all of the configurations tested and, therefore, differences between the results for the various geometrical modifications should still be meaningful. Details of the models with circumferential rectangular grooves are shown in Fig. 2 and given in Table 1.

Several of the models were tested with boundary-layer trips mounted ahead of the shoulder region. The trips were two-dimensional wires mounted at various locations along the body and varied in diameter from 0.63 to 0.99 mm. For a particular body configuration, there was little effect of changing the trip size or location. The exact trip used and trip location will be specified during the data presentations.

The afterbody modification using longitudinal V grooves consisted of four equally spaced grooves each with an included angle ($\theta_v$) of 90 deg. The angle $\theta_{BG}$ formed by the bottom of the V groove and the body centerline was 19.4 deg.

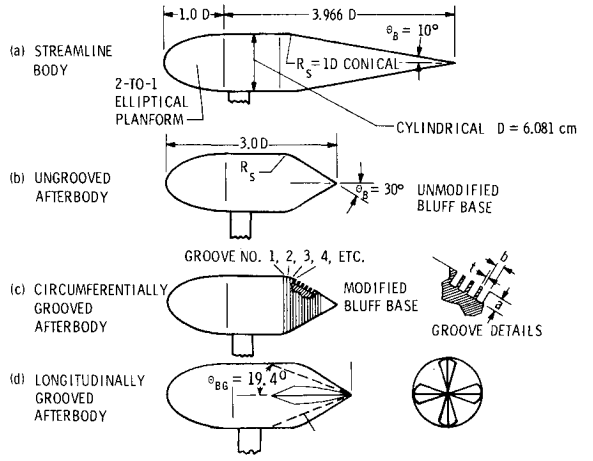


**Fig. 1 Examples of test configurations.**

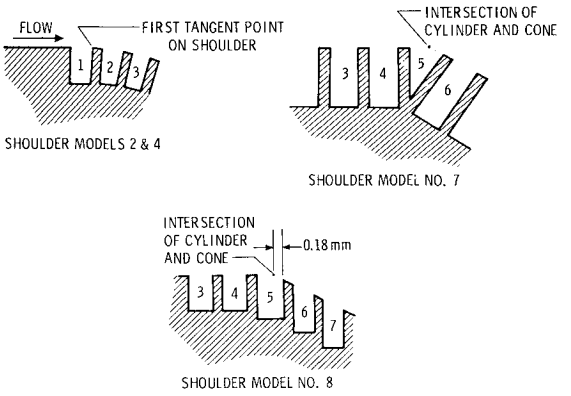


**Fig. 2 Details of the circumferentially (transverse) grooved afterbodies.**

**Table 1 Details of circumferential grooves[a]**

| | Surface distance ($S$), cm, for | | | | | | |
|---|---|---|---|---|---|---|---|
| | $R_sD=0$ | | $R_s/D=0.5$ | | $R_s/D=1.0$ | $R_s/D=1.5$ | $R_s/D=2.5$ |
| | Model 7 | Model 8 | Model 2 | Model 4 | Model 27 | Model 28 | Model 30 |
| | $a=0.203$<br>$b=0.102$<br>$t=0.025$ | $a=0.203$<br>$b=0.102$<br>$t=0.025$ | $a=0.203$<br>$b=0.102$<br>$t=0.025$ | $a=0.254$<br>$b=0.254$<br>$t=0.051$ | $a=0.203$<br>$b=0.102$<br>$t=0.102$ | $a=0.203$<br>$b=0.102$<br>$t=0.102$ | $a=0.203$<br>$b=0.102$<br>$t=0.102$ |
| Groove No. | $S=$ | $S=$ | $S=$ | $S=$ | $S=$ | $S=$ | $S=$ |
| 1 | −0.457 | −0.490 | 0.000 | 0.000 | 0.503 | 0.653 | 0.686 |
| 2 | −0.330 | −0.363 | 0.127 | 0.305 | 0.706 | 0.856 | 0.889 |
| 3 | −0.203 | −0.236 | 0.254 | 0.610 | 0.909 | 1.059 | 1.092 |
| 4 | −0.076 | −0.109 | 0.381 | 0.914 | 1.113 | 1.263 | 1.295 |
| 5 | 0.051 | 0.018 | 0.508 | 1.219 | 1.316 | 1.466 | 1.499 |
| 6 | 0.178 | 0.165 | 0.635 | 1.524 | 1.519 | 1.669 | 1.702 |
| 7 | 0.305 | 0.312 | 0.762 | 1.829 | 1.722 | 1.872 | 1.905 |
| 8 | 0.432 | 0.457 | 0.889 | 2.134 | 1.925 | 2.075 | 2.108 |
| 9 | 0.559 | 0.605 | 1.016 | 2.438 | 2.129 | 2.278 | 2.311 |
| 10 | 0.686 | 0.752 | 1.143 | 2.743 | 2.332 | 2.532 | 2.515 |
| 11 | 0.813 | 0.899 | 1.270 | 3.048 | 2.535 | 2.685 | 2.718 |
| 12 | 0.940 | 1.044 | 1.397 | 3.353 | 2.738 | 2.888 | 2.921 |
| 13 | | | 1.524 | 3.658 | | | |
| 14 | | | 1.651 | 3.962 | | | |
| 15 | | | 1.778 | 4.267 | | | |
| 16 | | | 1.905 | 4.572 | | | |
| 17 | | | | 4.877 | | | |
| 18 | | | | 5.182 | | | |
| 19 | | | | 5.486 | | | |

[a]Except for model 8, grooves are cut perpendicular to local surface. Model 8 has grooves cut perpendicular to model centerline.

## Results and Discussion

### Smooth Afterbodies with Shoulder Radiusing

The nominal minimum-drag configuration for a given bluff body is shaped such that the boundary layer remains attached on the entire surface, including the afterbody. Such a configuration is the "streamline" body shown in Fig. 1a. This body utilizes a gradual afterbody closure and a radius of $R_s/D=1.0$ at the shoulder to minimize the pressure-gradient effects that would separate the boundary layer on smaller fineness ratio bodies.

In some practical applications, gradual afterbody closure (such as that for the streamline body of the present study) results in excessive vehicle length; therefore a more rapid closure of the body is required (Fig. 1b). The major parameter which governs flow separation is the magnitude and extent of the longitudinal adverse pressure gradient ($dp/dx$) for a given flow condition. If the shoulder radius ($R_s/D$) of a highly truncated afterbody is small, then the longitudinal pressure gradient becomes quite large. One obvious approach to reduce the pressure gradient and thus retard separation is shoulder radiusing.[14-19] As the radius is made larger the pressure gradient becomes less severe and the flow remains attached further around the shoulder region. This, of course, reduces the base drag and thus the total drag as shown in Fig. 3 where the bluff afterbody shoulder radius ($R_s/D$) varied from 0 to 2.75. Also indicated in the figure is that, for a given radius, the flow remains attached over a greater distance as the energy in the boundary layer is increased with higher velocity or $Re$. For comparison, the drag on the streamline body ($F=5.0$) is also shown in Fig. 3.

Flow visualization, shown in Fig. 4, indicates that the boundary layer on the afterbody with $R_s/D=0$ separates immediately at the shoulder and does not reattach on the afterbody. For $R_s/D\geq 1.5$, the base drag appears to approach a limiting value and, at the higher $Re_D$, the afterbody with $R_s/D=2.00$ (and large closure angle of 30 deg) has approximately the same $C_D$ level as the streamline body. This favorable influence of afterbody shoulder radiusing was expected since previous research had indicated that shoulder radiusing was an effective method for reducing base drag of axisymmetric bluff bodies.[14-19] The effects of shoulder radiusing shown in Fig. 3 are directly related to the mitigating effects of shoulder radius increases upon pressure gradient.

As is well known, if the boundary layer is turbulent at the shoulder, it can be expected to tolerate larger gradients on a smaller shoulder radius before separating. Therefore, it is important to examine the effects of tripping the boundary layer. The effects of boundary-layer tripping ahead of the smooth conical afterbody were determined by placing a 0.863-mm-diam wire ring on the nose of the bluff body 2.03 cm from the stagnation point, measured along the surface. The drag data shown in Fig. 5 for this tripped boundary-layer configuration are compared to the untripped (laminar) configuration. For afterbodies where $R_s/D>0$, boundary-layer tripping helps to keep the flow attached at lower $Re_D$, but the trip produces a significant drag penalty at the higher $Re_D$ for $R_s/D=2.75$. The most important result shown in Fig. 5 is that the tripped boundary layer still separates as easily as a laminar boundary layer for an afterbody with $R_s/D=0$. Therefore, the $R_s/D=0$ case probably will benefit the most from geometrical modification to bluff afterbodies such as the circumferential rectangular or longitudinal V grooves to be discussed in the next two sections, respectively.

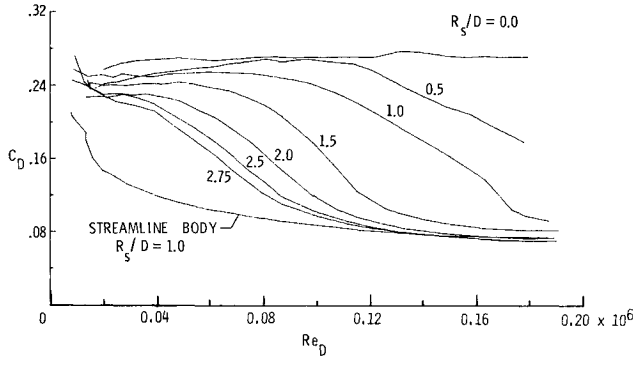


**Fig. 3 Afterbody drag variation with shoulder radius.**

### Circumferential Rectangular Grooves

The concept of using transverse surface grooves for delaying separation in diffusers evidently originated in the Soviet Union.[25-30] Research discussed in Refs. 12 and 31-33 also in-

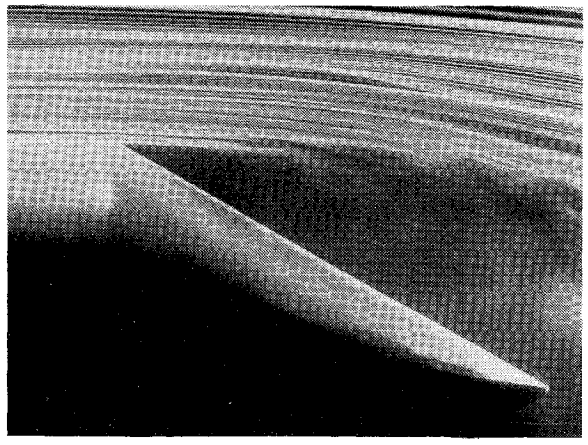

**Fig. 4 Flow visualization for ungrooved afterbody with $R_s/D=0$, $Re_D\simeq 62{,}000$, profile view of shoulder.**

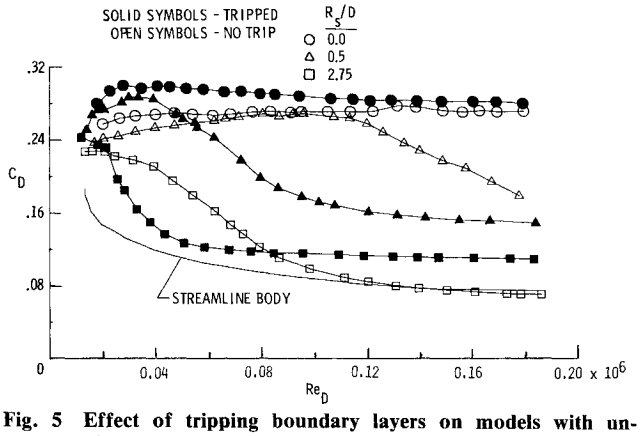


**Fig. 5 Effect of tripping boundary layers on models with ungrooved afterbodies and $R_s/D=0$ to 2.75.**

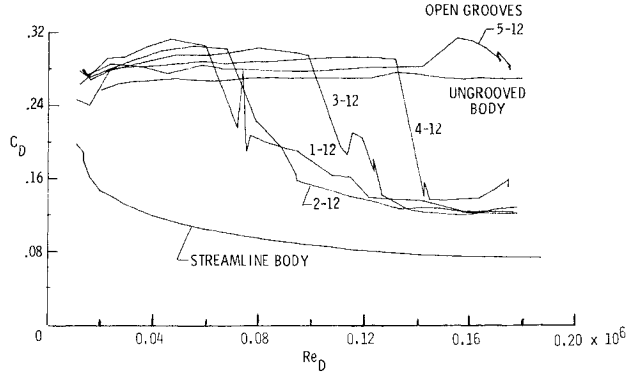


**Fig. 6 Influence of initial circumferential groove location on drag for afterbody with $R_s/D=0$; model 7.**

dicates that grooves are effective in controlling separation. References 25 and 30 suggest that the grooves function similar to a "roller bearing." However, there are at least three other mechanisms by which transverse grooves might affect afterbody base drag; i.e., 1) the grooves may shed vorticity which "energizes" the flow in the boundary layer,[34] 2) the groove at the shoulder may increase the effective shoulder radius locally, and 3) the grooves may act as a boundary-layer trip. In the present paper, the effect of grooving[20] the afterbody circumferentially on axisymmetrical bluff-body drag will be examined with zero and nonzero shoulder radius. The influence of the boundary-layer state at the shoulder of the afterbody will be explored also. Variation in the number of open grooves on the circumferentially grooved afterbodies was obtained by filling in selected grooves with dental plaster.

#### Circumferentially Grooved Afterbodies, $R_s/D=0$

The influence of circumferential grooves on the drag of an $R_s/D=0$ afterbody is shown in Fig. 6. The groove dimensions (model 7) and location relative to the shoulder are shown in Fig. 2 and Table 1. The rectangular grooves are perpendicular to the surface with one circumferential V groove centered around the shoulder. The data indicate that grooves located at or downstream of the shoulder (i.e., grooves 5-12) had no drag-reduction effect on the afterbody base drag; however, as the grooves ahead of the shoulder are opened, a reduction in drag occurs at lower $Re_D$. The beneficial effect of the upstream grooves reaches an asymptotic level around the first or second groove.

Two groove orientations were examined: grooves perpendicular to the surface (model 7) and grooves perpendicular to the model centerline (model 8). Although not shown here, the results indicated that the grooves perpendicular to the local surface were superior in reducing drag at the high test $Re_D$ (see Ref. 20).

The influence of a tripped boundary layer on the drag-reduction effectiveness of a grooved afterbody (model 7) with $R_s/D=0$ is examined in Fig. 7. The boundary-layer trip was a 0.99-mm-diam wire located 7.62 cm from the forebody stagnation point measured along the surface. The drag levels for the tripped boundary layer on the smooth ungrooved conical afterbody are also shown. The data indicate that the trip on the grooved body lowers the drag at lower $Re_D$ but produces a drag penalty at the higher $Re_D$. A comparison of the grooved and ungrooved afterbodies shows that the grooves can reduce the drag 35 and 54% for tripped and untripped (laminar) boundary layers, respectively. This is particularly important since this indicates that the circumferential grooves may be effective for the higher $Re_D$ case.

#### Circumferentially Grooved Afterbodies, $R_s/D>0$

Figures 8 and 9 present the drag data for circumferentially grooved afterbodies having a shoulder radius of $R_s/D=0.5$. Details of these grooves are shown in Table 1 and Fig. 2. The downstream side of the first groove coincided with the upstream tangency point of the shoulder radius. Also, groove 13 (model 2) roughly corresponds to the second tangency point of the shoulder radius. Figure 8 shows the drag reductions obtained by opening successive grooves downstream of the first tangency point. As the second tangency point is approached, the drag approaches an asymptotic limit for a given $Re_D$. It should be noted that the first three grooves on model 2 actually increase the drag over certain $Re_D$ ranges. The beneficial effect of the grooves on separation is not sufficient to overcome the drag penalty of the grooves. Results for different size grooves (model 4) were similar to those for model 2 and are not shown.

Figure 9 examines the influence of the grooves near the first tangency point when the downstream grooves are opened. The data for grooves 7-13 on model 2 indicate the

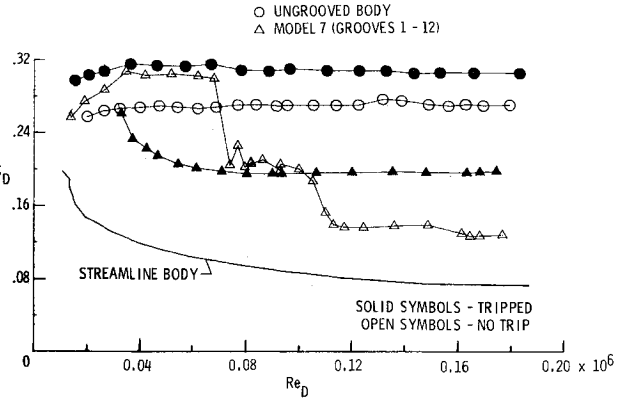


**Fig. 7 Effect of tripping boundary layer on a circumferentially grooved afterbody with $R_s/D=0$.**

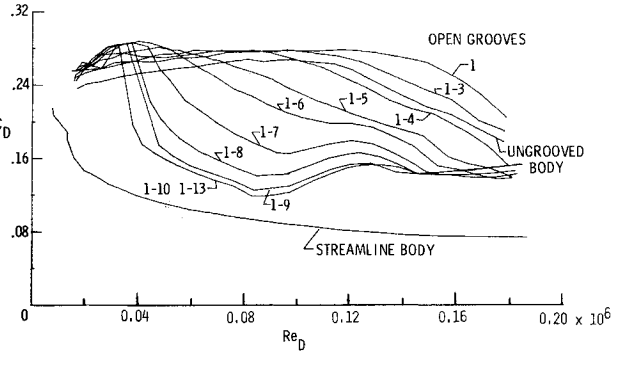


**Fig. 8 Influence of number of circumferential grooves on afterbody drag with $R_s/D=0.5$; model 2.**

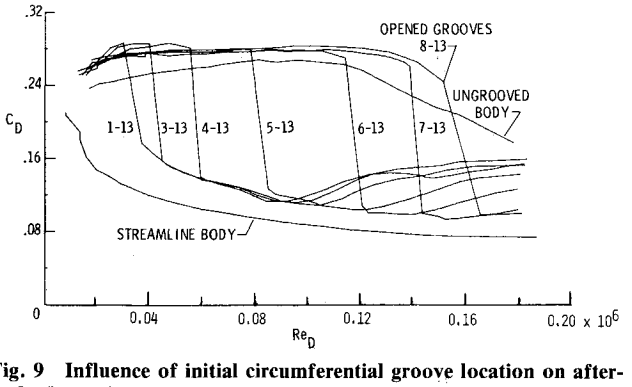


**Fig. 9 Influence of initial circumferential groove location on afterbody drag with $R_s/D=0.5$; model 2.**

drag reductions can be obtained with the first open groove located downstream of the first tangency point. As the first opened groove approaches the first tangency point, drag reduction is obtained at lower values of $Re_D$. As $Re_D$ is increased the boundary layer becomes thinner and remains attached further around the shoulder before separating. It is near this separation point where the grooves evidently should be placed.

Flow-visualization photographs for the grooved and ungrooved afterbodies with $R_s/D=0.5$ are shown in Fig. 10 for $Re_D \simeq 50{,}000$. The ungrooved afterbody configuration in Fig. 10a indicates no turning of the streamlines, boundary-layer separation just downstream of the first tangency point, and no flow reattachment of the afterbody. This large region of afterbody separation corresponds to the high drag levels shown in Figs. 8 and 9 for the ungrooved afterbody with $R_s/D=0.5$. Figure 10b shows that grooves placed between the tangency points of the shoulder radius turn the stream-

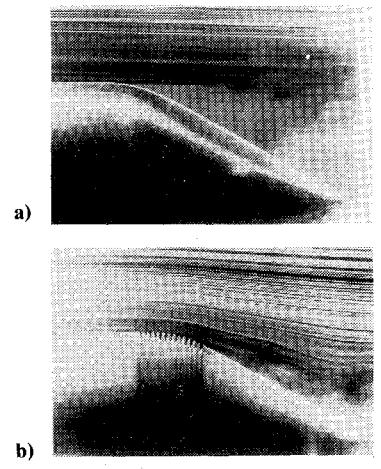


**Fig. 10 Flow visualization for afterbodies with $R_s/D=0.5$, $R_e/D\simeq 50{,}000$, profile view of shoulder: a) ungrooved afterbody, and b) model 2, open grooves 1-13.**

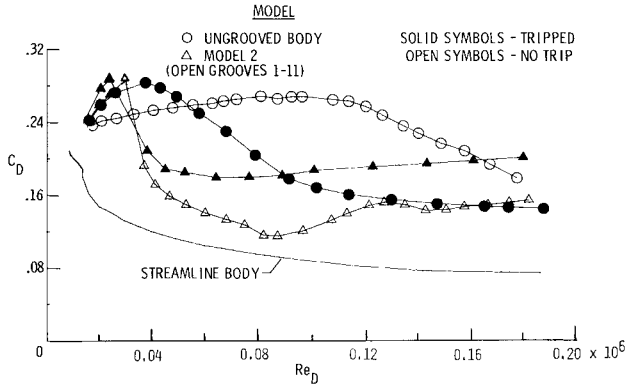


**Fig. 11 Tripped boundary layer on a circumferentially grooved afterbody with $R_s/D=0.5$.**

lines, move the separation point downstream, and greatly decrease the regions of afterbody base separation.

It is believed from the interpretation of the flow-visualization results (all flow-visualization results are not shown here) that the dominant effect of the circumferential grooves is to trade the large region of separated flow over the ungrooved afterbody for smaller regions of separated flow that occur in the indivdual grooves, i.e., a "slip" wall boundary condition is imposed on the flow. It appeared from the visualization results that the flow in the grooves was relatively quiescent in the present tests, i.e., the grooves did not act as a boundary-layer trip. Before the boundary layer is able to separate and form a large separated base region, it separates over the grooved cavity and forms a smaller region of separation in the cavity. Downstream of the cavity, the flow appears to reattach on the fin or land separating the two grooves. Before the boundary layer is able to thicken, separate, and form a large base separation region, the second groove or cavity is encountered. In this manner, the boundary layer on the afterbody is kept thin which helps to keep the flow attached and the separation regions small.

The influence of boundary-layer tripping on the circumferentially grooved afterbody with $R_s/D=0.5$ (model 2) is given in Fig. 11. The boundary-layer trip was a 0.635-mm-diam wire located 2.03 cm from the forebody stagnation point measured along the surface. Drag data for a tripped boundary layer on the ungrooved afterbody with $R_s/D=0.5$ are also shown for comparison. Except for low $Re_D$, the data indicate that the circumferential grooves are effective

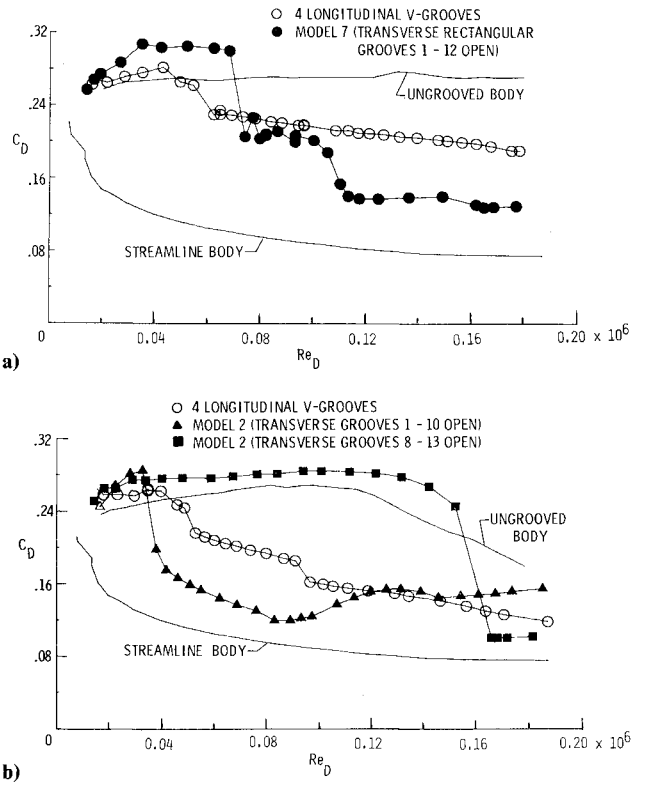


**Fig. 12 Longitudinal V grooves compared to circumferential (transverse) rectangular grooves: a) $R_s/D=0$: and b) $R_s/D=0.5$.**

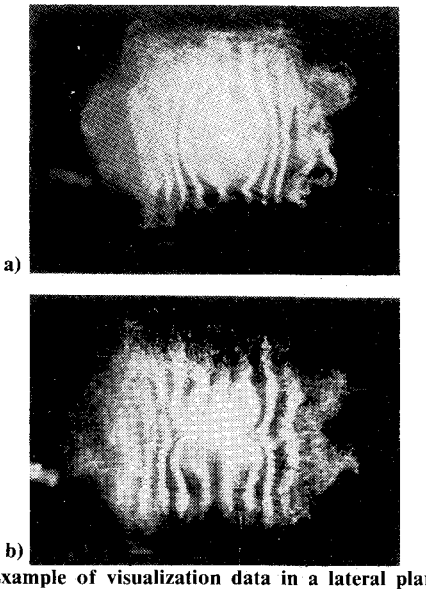


**Fig. 13 Example of visualization data in a lateral plane near the base apex, rear view of base apex: a) without grooves and b) with longitudinal V grooves.**

only if the boundary layer ahead of the shoulder is laminar, as in the untripped case. At the higher $Re_D$, the grooves produce an increase in drag for the tripped boundary layer.

Although not shown here, the drag results on models where $R_s/D=1.0$, 1.5, and 2.5 (see Table 1) indicated that the effectiveness of circumferential grooves, even for a laminar boundary layer, is greatly diminished at the higher values of $R_s/D$ approaching 1.5, i.e., the grooves can be used in lieu of shoulder radiusing. Therefore, indications are that circumferential grooves will have application only to bodies where $R_s/D<1.0$.

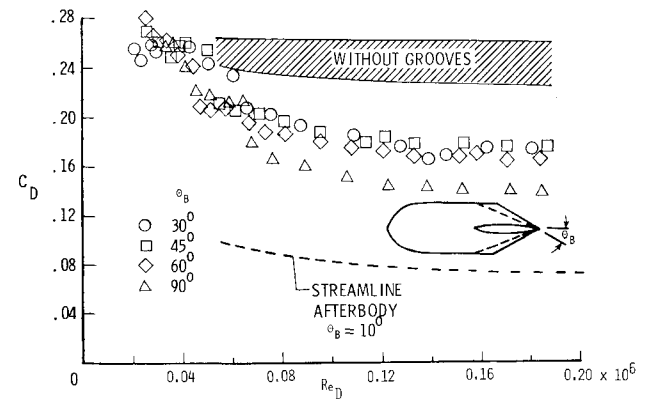


**Fig. 14 Effect of $\theta_B$ for longitudinally V-grooved afterbody $R_s/D=0$.**

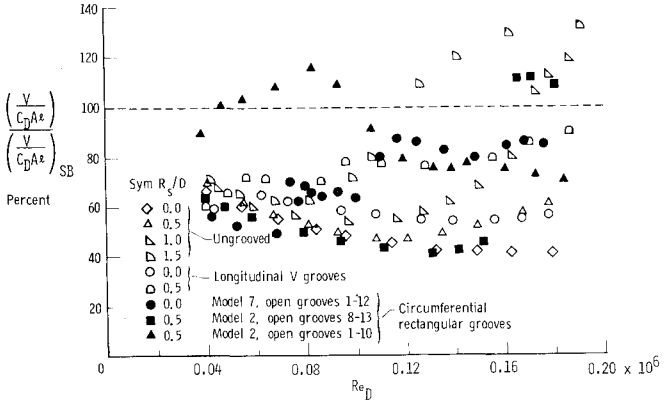


**Fig. 15 Drag and volumetric efficiency for grooved and ungrooved afterbodies.**

### Longitudinal V Grooves

An example of an afterbody with four longitudinal V grooves is shown in Fig. 1d. Examples of drag reduction that can be achieved by use of longitudinal V grooves[18,21] cut through the bluff afterbody shoulder region are shown for $R_s/D=0$ and 0.5 in Fig. 12, where a comparison is made with the transverse grooves discussed previously.

The mechanism believed to cause this reduction is illustrated by comparing cross-sectional smoke-flow patterns for a longitudinal station near the apex of the conical base (see Fig. 13). These flow-visualization data indicate that the smoke lines continue to be bowed outward as they pass the apex of the smooth (ungrooved) afterbody. However, a very noticeable difference occur, when grooves are employed. Figure 13b shows that the smoke lines are drawn inward in the region of the V grooves suggesting that the flow remains attached in the grooves. Furthermore, the residual separated-flow regions on the grooved model (Fig. 13b) are of considerably smaller extent than the corresponding pie-shaped sections on the smooth model (Fig. 13a). These visualization results suggest the following drag-reduction mechanism: the bottoms of the grooves (which begin upstream of the shoulder) have a much smaller afterbody closure angle (19.4 deg) than the surface of the afterbody (30 deg). Therefore, the flow in the grooves remains attached and probably provides an ejector-like pumping action for the remaining, fully three-dimensional, separated-flow segments of the afterbody. Such ejector-like action is probably also provided by the side-edge vortices.

Up to this point all bluff afterbodies discussed had a closure angle $\theta_B$ of 30 deg. However, during the study[18] of longitudinal V grooves, additional closure angles of 45, 60, and 90 deg were investigated with $R_s/D$ varing from 0 to 1.5. The V grooves generally reduced drag for all combinations of closure angles and shoulder radii when $\theta_{BG}$ (the closure angle of the V groove) was 19.4 deg. Also, drag was decreased slightly for $R_s/D=0$ as the closure angle increased from 30 to 90 deg for both the grooved and ungrooved cases. This effect diminished as $R_s/D$ was increased from 0 to 1.5. For the ungrooved case, this is in agreement with the well-known "Kammback" principle (i.e., only slight effect of closure angle on drag once separation has occurred). The slight decrease (see Fig. 14) in drag with increase in $\theta_B$ on the grooved models is probably at least partially due to the decrease in the remaining axially projected base surface area.

### Volumetric Efficiency with and without Grooves

It is quite obvious that if drag is reduced by either type of groove or by increasing the shoulder radius, the available volume is decreased. Therefore, some of the data will now be compared on a volumetric efficiency basis. It is assumed herein that a suitable measure of volumetric efficiency is the body volume per unit of drag force. The dimensionless parameter $V/C_DA\ell$ for a bluff body ($\ell/D=3.0$) is ratioed to that for the streamline body ($\ell/D=4.966$) in Fig. 15. Note that $V/\ell$ is the volumetrically effective cross-sectional area. The figure shows that although both types of grooves can produce some improvement (over the ungrooved case) in the volumetric efficiency, a larger improvement occurs from the shoulder radiusing at the higher range of $Re$ tested.

Unanswered questions include 1) How would these afterbody modifications compare at much higher $Re$?; 2) What would be the effect if the boundary layer were naturally fully turbulent?; 3) How would combining the circumferential and longitudinal grooves or skewing the grooves affect the results? Further tests are needed to answer these questions.

## Concluding Remarks

Experimental investigations were conducted to determine if there are conditions under which geometric modifications to the aft shoulder region would reduce drag on highly truncated bluff bodies for a range of Reynolds numbers based on body diameter ($Re_D$) between 20,000 and 200,00.

The results indicated the following:

1) For $Re_D > 100{,}000$, shoulder radiusing ($R_s$) relative to body diameter ($D$) of $R_s/D=2.00$ was found to reduce the body drag to levels equivalent to a streamline body having 67% greater fineness ratio. The drag reduction is accomplished through a reduction of the adverse pressure gradient ($dp/dx$).

2) Circumferential grooves cut perpendicular to the local surface were found to provide net body drag reductions on the order of 50 and 35% with zero shoulder radius for laminar and tripped boundary layers, respectively.

3) For $R_s/D=0.5$, circumferential grooves are effective only for laminar boundary layers approaching the shoulder.

4) The data indicate that, to be effective, the circumferential grooves must be located in the region where the longitudinal pressure gradient is sufficiently large to cause separation.

5) The major drag-reduction mechanism of the circumferential grooves appears to be one of substituting several smaller regions of separation for a larger separated-flow region (e.g., obviate the usual no-slip boundary condition).

6) Application of the circumferential grooves to afterbodies where the flow remains attached for some reason generally results in a drag penalty.

7) The V grooves are most effective in reducing drag when the afterbody shoulder radius is zero. Reductions in drag on the order of 33% were measured for this condition.

8) The longitudinal grooves are effective only at the lower Reynolds numbers of the present tests for large shoulder radius.

9) The drag-reduction mechanisms for longitudinal V grooves appears to be associated with a) attached flow in the grooves, and b) the ejector (pumping) action of the attached groove flow on residual (highly three-dimensional) separated flow regions.

10) Afterbody shoulder radiusing appears to be a more efficient technique for reducing bluff-body base drag than either circumferential or longitudinal grooving except at the lower $Re_D$.

## References

[1]"Vehicle Aerodynamics: The Next Fuel Economy Frontier," *Automative Engineering,* Vol. 86, July 1978, pp. 19-24.

[2]Hefner, J. N. and Bushnell, D. M., *An Overview of Concepts for Aircraft Drag Reduction,* AGARD Rept. 654, 1977, 1-1—1-30.

[3]Mair, W. A., "Drag-Reduction Techniques for Axisymmetric Bluff Bodies," *Aerodynamic Drag Mechanisms of Bluff Bodies and Road Vehicles,* Plenum Press, New York, 1978, pp. 161-187.

[4]Gai, S. L. and Patil, S. R., "Subsonic Axisymmetric Base Flow Experiments with Base Modification," *Journal of Spacecraft and Rockets,* Vol. 17, Jan.-Feb. 1980, pp. 42-46.

[5]Kelly, M. W. and Tolhurst, W. H. Jr., "Full-Scale Wind-Tunnel Test of a 35° Sweptback Wing Airplane with High-Velocity Blowing over the Trailing-Edge Flaps," NACA RM-A55109, Nov. 1955.

[6]McLemore, C. H., and Pink, M. P., "Blowing Over the Flaps and Wings Leading Edge of a Thin 49° Swept-Body-Trail Configuration in Combination with Leading Edge Devices," NACA RM-L56E16, July 1956.

[7]Anderson, S. B., Quigley, H. C., and Innis, R. C., "Flight Measurements of the Low-Speed Characteristics of a 35° Swept-Wing Airplane with Blowing-Type Boundary-Layer Control on the Trailing-Edge Flaps," NACA RM-A56G30, Oct. 1956.

[8]Maki, R. L., "Low Speed Wind-Tunnel Investigation of Blowing Boundary-Layer Control on Leading- and Trailing-Edge Flaps of a Large-Scale, Low-Aspect Ratio, 45° Swept Wing Airplane Configuration," NASA Memo 1-23-59A, Jan. 1959.

[9]Maki, R. L. and Giulianetti, D. J., "Low-Speed Wind Tunnel Investigation of Blowing Boundary-Layer Control on Leading- and Trailing-Edge Flaps of a Full-Scale, Low-Aspect-Ratio, 42° Swept-Wing Airplane Configuration," NASA TN D-16, Aug. 1959.

[10]Quigley, H. C. and Hom, F. W. K., "A Flight Investigation of Aera Suction and Blowing Boundary-Layer Control on the Trailing-Edge Flaps of a 35° Swept-Wing Carrier-Type Airplane," NACA RM-A57B14, April 1957.

[11]Lachmann, G. V., *Boundary Layer and Flow Control—Vol. I,* Pergamon Press, New York, 1961.

[12]Chang, P. K., *Control of Separation,* Hemisphere Publishing Corp., McGraw-Hill Book Co., New York, 1976.

[13]Anderson, S. B., Faye, A. E. Jr., and Innis, R. C., "Flight Investigation of the Low-Speed Characteristics of a 35° Swept Wing Airplane Equipped with an Area Suction Ejector Flap and Various Wing Leading Edge Devices," NACA RM-A57G10, Sept. 1957.

[14]Silhan, F. V. and Cubbabe, J. M. Jr., "Drag of Conical and Circular-Arc Boattail Afterbodies at Mach Numbers from 0.6 to 1.3," NACA RM-L57L22, 1957.

[15]Shrewsbury, G. D., "Effect of Boattail Junction Shape on Pressure-Drag Coefficients of Isolated Afterbodies," NASA TM X-15167, March 1968.

[16]Mair, W. A., "Reduction of Base Drag by Boattailed Afterbodies in Low-Speed Flow," *The Aeronautical Quarterly,* Vol. XX, Nov. 1969, pp. 307-320.

[17]Payne, P. R., Hartley, R. M., and Taylor, R. M., *Afterbody Drag: Vol. 1—Drag of Conical and Circular-Arc Afterbodies Without Jet Flow,* DTNSRDC/ASED-80/10, May 1980.

[18]Howard, F. G., Quass, B. F., Weinstein, L. M., and Bushnell, D. M., "Longitudinal Afterbody Grooves and Shoulder Radiusing for Low-Speed Bluff Body Drag Reduction," ASME Paper 81-WA/FE-5, Nov. 1981.

[19]*Aerodynamic Drag Mechanisms of Bluff Bodies and Road Vehicles,* edited by G. Sovran, T. Morel, and W. Mason, Plenum Press, New York, 1978.

[20]Howard, F. G., Goodman, W. L., and Walsh, M. J., "Axisymmetric Bluff-Body Drag Reduction Using Circumferential Grooves," AIAA Paper 83-1788, July 1983.

[21]Quass, B., Howard, F. G., Weinstein, L. M., and Bushnell, D. M., "Longitudinal Grooves for Bluff Body Drag Reduction," *AIAA Journal,* Vol. 19, April 1981, p. 535.

[22]Wilkinson, S. P., "An Experimental Investigation of a Turbulent Boundary Layer with Suction Through Closely-Spaced Streamwise Slots," M.S. Thesis, Old Dominion University, Norfolk, Va., 1978.

[23]Corke, T., Koga, D., Drubka, R., and Nagib, H., "A New Technique for Introducing Controlled Sheets of Smoke Streaklines in Wind Tunnels," *Proceedings of International Congress on Instrumentation in Aerospace Simulation Facilities,* IEEE Pub. 77, CHI261-18 AES, 1977, p. 74.

[24]Sykes, D. M., "Blockage Corrections for Large Bluff Bodies in Wind Tunnels," *Advances in Road Vehicle Aerodynamics 1973,* edited by H. S. Stephens, BHRA Fluid Engineering, Cranfield, England, pp. 311-322.

[25]Migay, V. K., "The Efficiency of Cross Ribbed Curvilinear Diffuser," *Energomashinostroennie,* No. 1, 1962, pp. 45-46.

[26]Migay, V. K., "The Aerodynamic Effectiveness of a Discontinuous Surface," *Inzhenerno-Fizicheskiy Zhurnal,* Vol. 5, No. 4, 1962, pp. 20-24.

[27]Migay, V. K., "Diffuser with Transverse Fins," *Energomashinostroyeniye,* No. 4, 1960, p. 32.

[28]Migay, V. K., "On Improving the Effectiveness of Diffuser Flows with Separation," *Mekhanika i mashinostroyeniye,* No. 4, 1960, pp. 171-173.

[29]Migay, V. K., "Increase of Diffuser Efficiency by Means of Transverse Fins," *Teploenergetika,* Vol. 8, No. 4, 1961, pp. 41-43.

[30]Migay, V. K., "A Study of Finned Diffusers," *Teploenergetika,* No. 10, 1962, pp. 55-59.

[31]Stull, F. D. and Velkoff, H. R., "Flow Regimes in Two-Dimensional Ribbed Diffusers," *Journal of Fluids Engineering,* Vol. 97, No. 1, March 1975, pp. 87-96.

[32]Stull, F. D., and Velkoff, H. L., "Effects of Transverse Ribs on Pressure Recovery in Two-Dimensional Subsonic Diffusers," AIAA Paper 72-1141, Nov.-Dec. 1972.

[33]Stull, F. D., Curray, E. T., and Valkoff, H. R., "Investigation of Two-Dimensional Cavity Diffusers," AFAPL-TR-73-84, Oct. 1973.

[34]Morozov, M. G., "Investigation of the General Characteristics of Supersonic Vortex Boundary Layers," *Inzhenerno-Fizicheskii Zhurnal,* Vol. 22, May 1972, pp. 885-889.